Non-Linear Phase Noise Mitigation over Systems using Constellation Shaping

Grid-Forming Inverter with Simplified Virtual Synchronous Compensator Providing Grid Services and Grid Support

Vincenzo Mallemaci
Dipartimento Energia 'Galileo Ferraris'
Politecnico di Torino
Torino, 10129, Italy
vincenzo.mallemaci@polito.it

Enrico Carpaneto
Dipartimento Energia 'Galileo Ferraris'
Politecnico di Torino
Torino, 10129, Italy
enrico.carpaneto@polito.it

Radu Bojoi
Dipartimento Energia 'Galileo Ferraris'
Politecnico di Torino
Torino, 10129, Italy
radu.bojoi@polito.it

***Abstract*—This paper proposes a Simplified Virtual Synchronous Compensator (S–VSC) model with grid–forming capabilities for microgrid applications. Previous works have shown how the S–VSC can provide grid services (i.e., virtual inertia, current harmonic compensation and reactive support during faults) in grid–feeding configuration. In this paper, the S–VSC model is extended to a grid–forming converter to demonstrate its capability to work in island as well, thus representing a promising solution for the control of a microgrid. The control algorithm is validated on a 15 kVA inverter connected to a scaled microgrid.**

***Index Terms*—virtual synchronous machine, virtual synchronous compensator, microgrid, grid forming**

I. Introduction

In the present years, the power system is facing a transition from the centralized energy production to the distributed generation, especially from renewable energy sources (RESs). In this context, the diffusion of microgrids (MGs) represents a valid solution to integrate more efficiently the distributed energy resources [1]–[3]. However, a predominance of inverter–interfaced energy sources would reduce the total inertia and compromise the voltage stability of the power system. To face these issues, renewable–energy power plants will be required to provide grid services (e.g., inertial behavior, harmonic compensation), grid support, as well as operation in island mode [4], [5]. Unfortunately, standard control techniques for RESs (i.e., Maximum Power Point Tracking) are not suitable to guarantee the provision of such services. To overcome this limitation, a promising method is to control grid inverters to make them emulate the behavior of conventional synchronous generators, and even outperform them. Many solutions have been proposed in the last years under the name of Virtual Synchronous Machines (VSMs) [6]–[16]. A promising solution is the S–VSC model [17]–[22], which operates as a synchronous compensator, only in charge of the provision of the grid services, leaving the power generation to the classical inverter structure. However, this model has been validated in previous works only for grid–tied operation [20], with no discussion on its grid–forming capabilities and island operation. Therefore, this paper proposes a grid–forming S–VSC model, which can represent a valid solution for inverter–based MGs.

This paper is divided as follows. In Section II the original structure of the S–VSC model is briefly described together with the scaled microgrid under study. In Section III the grid–forming S–VSC model is presented. The experimental validation of the control is proposed in Section IV. Finally, the conclusions of this work are provided in Section V.

II. S–VSC Model

A block scheme of the microgrid under study is illustrated in Fig. 1. A three phase inverter is connected to the grid through

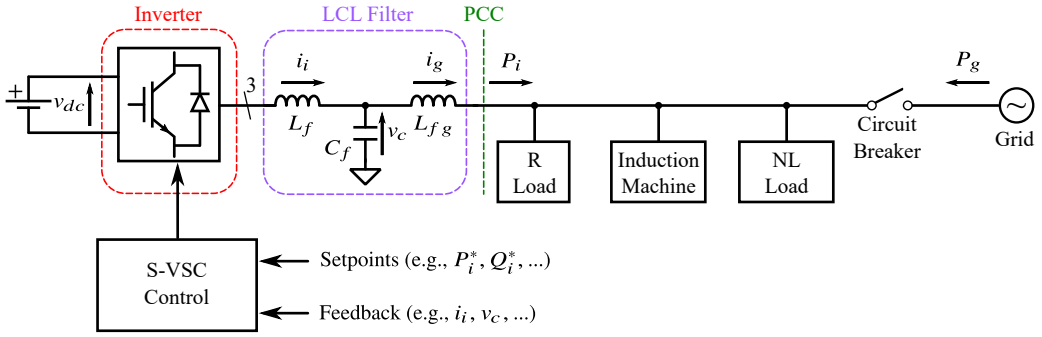

Fig. 1. Block scheme of the microgrid under study.

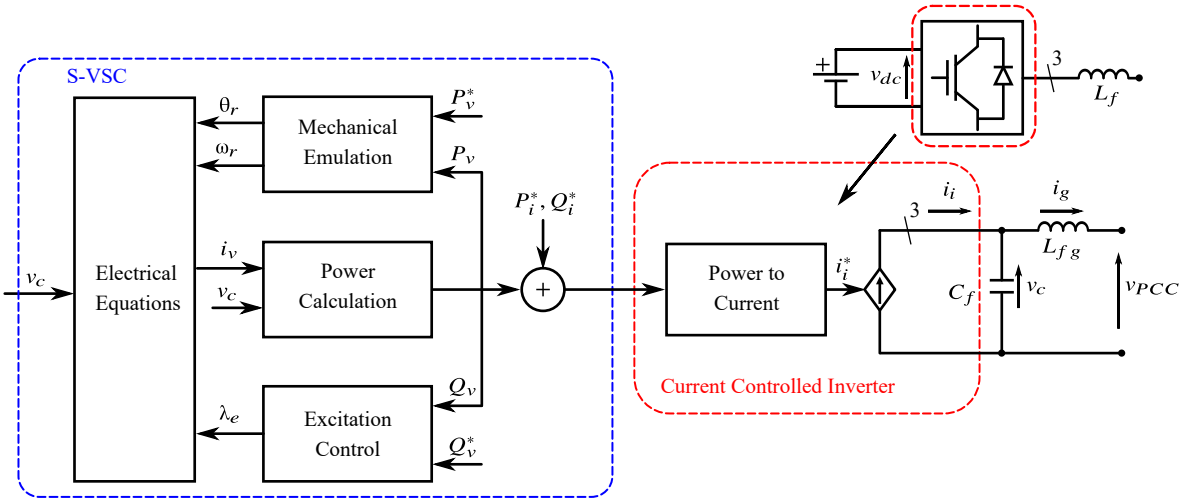

Fig. 2. Block scheme of the inverter controlled according to the S–VSC model.

an LCL filter. At the point of common coupling (PCC), three loads are connected: a resistive load (R load), an induction machine (IM) and a non linear load (NL load). Finally, a circuit breaker connects the PCC and the grid. The inverter is supplied by a dc–source and it is controlled according to the S–VSC control algorithm.

The S–VSC is a voltage–input, power–output virtual synchronous machine. Its block scheme is proposed in Fig. 2. All the quantities are in per unit (pu), referred to the base values listed in Table I. The S–VSC model consists of the following main blocks:

- *Electrical Equations*: it implements the S–VSC virtual stator equations. They provide the virtual current i_v starting from the measured capacitor voltage v_c, the virtual rotor position θ_r, the virtual rotor speed ω_r and the virtual excitation flux λ_e;
- *Mechanical Emulation*: it emulates the swing equation [23], i.e., the relationship which describes the mechanical behavior of the S–VSC model. It is used to retrieve both ω_r and θ_r from the virtual power P_v and the reference virtual power P_v^*;
- *Excitation Control*: this block regulates the excitation flux λ_e and the reactive power exchange with the grid [24].

The S–VSC can autonomously synchronize to the grid with no additional algorithms (e.g., phase locked loop) [20]. Finally, the inverter control is performed by means of the references P_i^* and Q_i^* and the virtual power references P_v^* and Q_v^* are used to provide ancillary services.

III. High Level Control

The original S–VSC model can be modified by adding a high level control highlighted in Fig. 3.

The high level control consists of two external control loops. The first one is the active droop control law, in charge of the proportional regulation of the frequency, during both grid–tied and island operation:

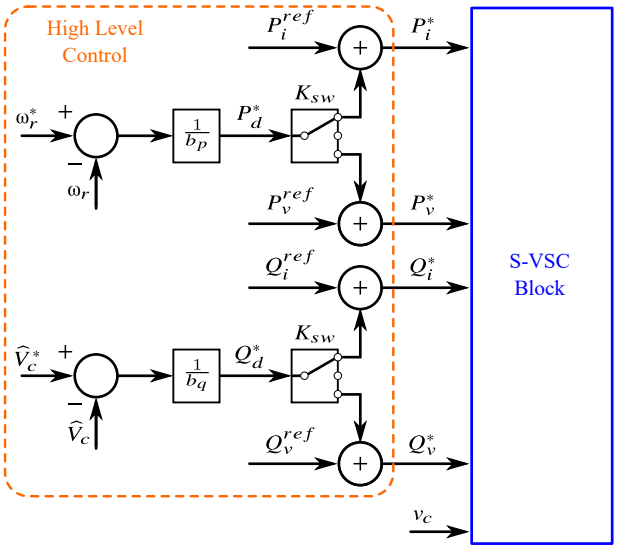

Fig. 3. Block scheme of the high level control.

$$P_d^* = \frac{\omega_r^* - \omega_r}{b_p} \tag{1}$$

where P_d^* is the reference of droop active power, ω_r^* is the speed reference and b_p is the active droop coefficient. This is set to the conventional value of 2% [23].

The second external controller is the reactive droop control law, responsible for the proportional regulation of the voltage amplitude $\widehat{V}_c$, during both grid–tied and island operation:

$$Q_d^* = \frac{\widehat{V}_c^* - \widehat{V}_c}{b_q} \tag{2}$$

where Q_d^* is the reference of droop reactive power, $\widehat{V}_c^*$ is the voltage reference and b_q is the reactive droop coefficient, set to the conventional value of 50% [23].

By adding these two external loops, the superior performance of the compensator operation with respect to classical VSMs is preserved [20], while adding the capability to operate in a MG as a grid–forming converter.

According to the multiport logical switch K_{sw} in Fig. 3, the two references P_d^* and Q_d^* can be:

- added to the inverter external references P_i^{ref} and Q_i^{ref};
- not used (i.e., the high level control is disabled);
- added to the virtual external references P_v^{ref} and Q_v^{ref}.

In this paper, the references P_d^* and Q_d^* are always added to the inverter external references, thus preserving the compensator operation.

IV. Experimental Validation

The S–VSC grid–forming capability is validated by means of two experimental tests. The scheme of the microgrid under analysis has been already illustrated in Fig. 1. Two pictures of the experimental setup are shown in Fig. 4a and Fig. 4b, while the main data are collected in Table I.

The inverter is supplied by a 15 kW dc–source and controlled by a dSPACE platform at a switching frequency f_{sw} = 10 kHz. Three kinds of loads are chosen to evaluate the behavior of the grid–forming S–VSC model in island operation: a linear load (R load), a rotating load (IM) and a non linear load (NL load). They can be connected and disconnected to the system through breakers. A starter is located between the IM and the PCC to limit the inrush current during the start up by imposing a maximum slew rate to the supply voltage. Moreover, the IM is loaded by a programmable mechanical load. The NL load is a three–phase diode rectifier connected at the PCC through a 0.09 pu inductive filter. At the dc–side, the rectifier is connected to a capacitor bank of 3.3 mF in parallel with an electronic constant power load set to 0.1 pu.

The two experimental tests are described as follows:

- Test 1: inverter external power references set to 0 pu. If the inverter is connected to the grid, the load power is provided by the grid and the inverter can only provide ancillary services. As soon as the microgrid is islanded, the inverter must immediately satisfy the load demand;
- Test 2: non–zero inverter external references (e.g., emulating renewable plant generation). The test starts in grid–tied operation. The reference P_i^{ref} changes over time (e.g., production change of a photovoltaic or wind power plant). As soon as the microgrid is islanded, the inverter must immediately inject the power requested by the load and follow the load changes.

In both tests the speed reference ω_r^* is set to the S–VSC frequency value (pu) after the inverter synchronization procedure (i.e., the grid frequency value in that instant). The same approach is applied for the voltage reference $\widehat{V}_c^*$, set to the measured amplitude $\widehat{V}_c$ after the synchronization procedure.

A. Test 1: Zero inverter external references

Fig. 5 shows the results of Test 1. The main events are summarized in Table II. During the first part, the three loads

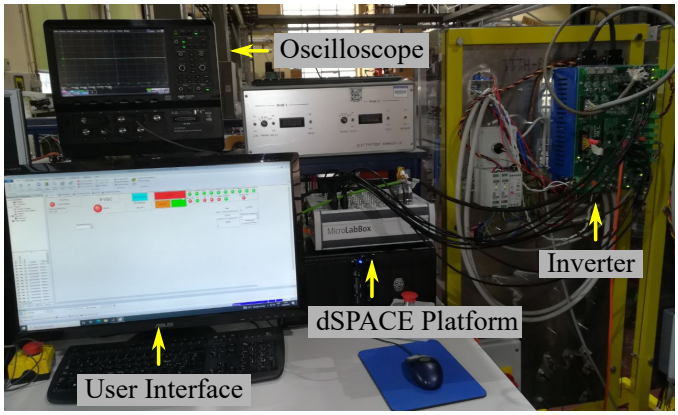

(a)

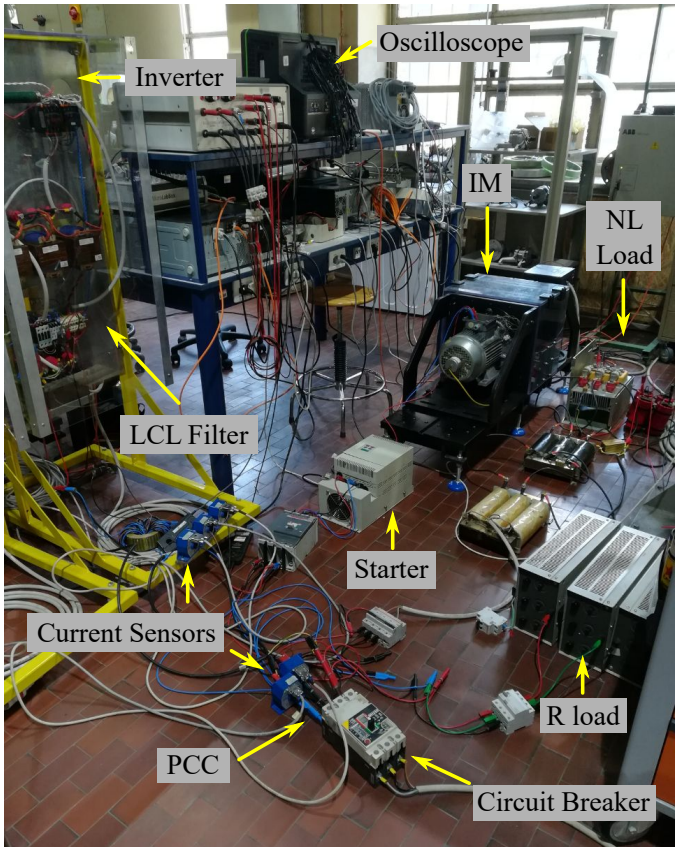

(b)

Fig. 4. Pictures of the experimental setup.

TABLE I
Main Data of the Experimental Setup.

Base Values		Inverter		LCL Filter	
S_b	15 kVA	S_N	15 kVA	L_f	0.060 pu
V_b	230 $\sqrt{2}$ V	I_N	30 A	C_f	0.017 pu
I_b	30 A	f_{sw}	10 kHz	L_{fg}	0.065 pu
Z_b	10.67 Ω	V_{dc}	380 V		
f_b	50 Hz				
Resistive Load		**Induction Machine**		**Non linear Load**	
P_N	0.1 pu	S_N	0.27 pu	P_N	0.1 pu

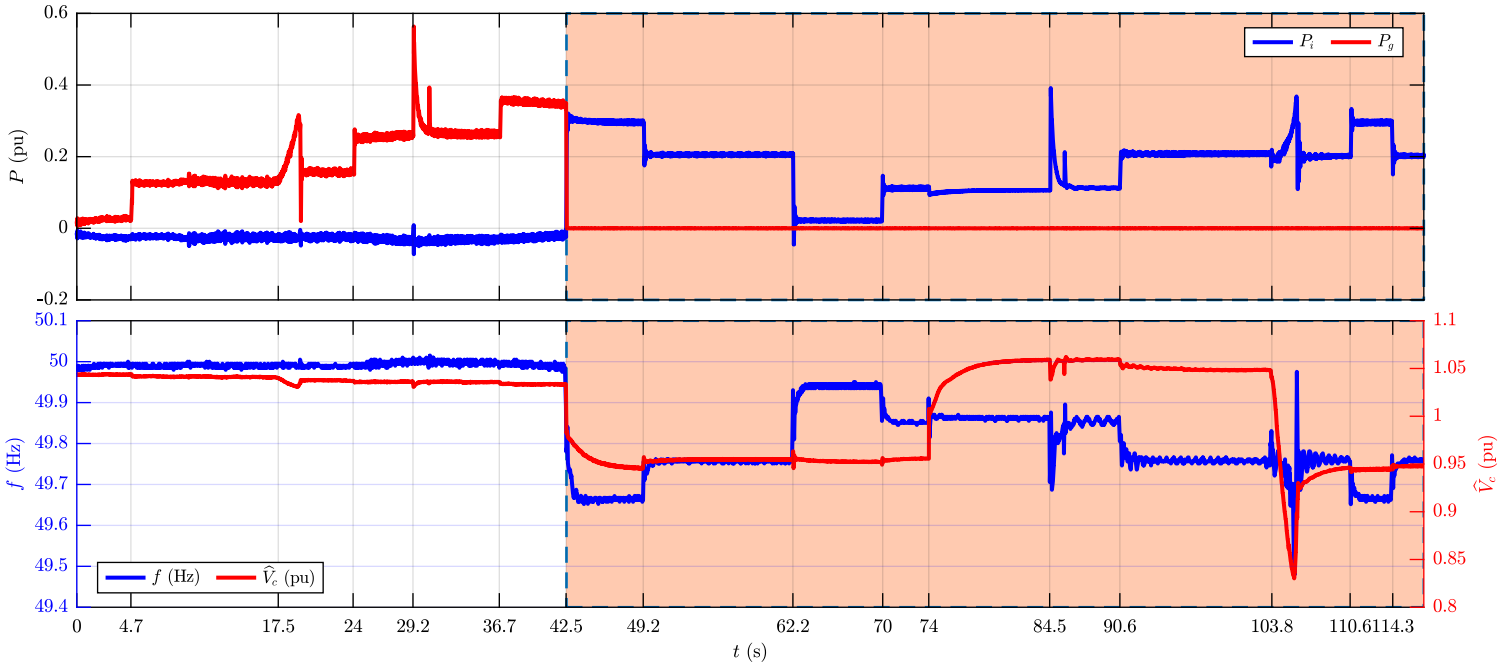

Fig. 5. Results of Test 1: (top) inverter power P_i (pu) and grid power P_g (pu) moving average trends; (bottom) S–VSC frequency f (Hz) and voltage amplitude $\widehat{V}_c$ (pu) trends.

TABLE II
EVENTS LIST OF TEST 1.

Time (s)	Comment
0	$f \neq 50$ Hz $\Rightarrow P_d^* \neq 0 \Rightarrow P_i \neq 0$.
4.7	R Load insertion $\Rightarrow \Delta P_g = 0.1$ pu.
17.5	IM start up. The starter limits the inrush current.
24	10 Nm IM load insertion $\Rightarrow \Delta P_g = 0.1$ pu.
29.2	NL load precharge.
36.7	NL load insertion $\Rightarrow \Delta P_g = 0.1$ pu.
42.5	The circuit breaker is opened: Islanding $\Rightarrow$ $\Rightarrow P_g = 0$ pu , $\Delta P_i = 0.3$ pu: the inverter immediately supplies the loads.
49.2	NL load disconnection $\Rightarrow \Delta P_i = -0.1$ pu.
62.2	IM torque inversion from 10 Nm to –10 Nm $\Rightarrow$ $\Rightarrow \Delta P_i = -0.2$ pu: the IM works as a generator and provides almost all the R load power.
70	IM torque load = 0 Nm $\Rightarrow \Delta P_i = 0.1$ pu: the inverter provides the power requested by the loads.
74	IM disconnection.
84.5	NL load precharge.
90.6	NL load insertion $\Rightarrow \Delta P_i = 0.1$ pu.
103.8	IM start up. The starter limits the inrush current.
110.6	10 Nm IM load insertion $\Rightarrow \Delta P_i = 0.1$ pu.
114.3	IM torque load = 0 Nm $\Rightarrow \Delta P_i = -0.1$ pu.

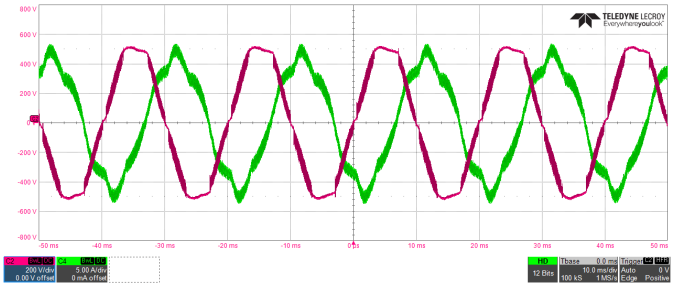

(a)

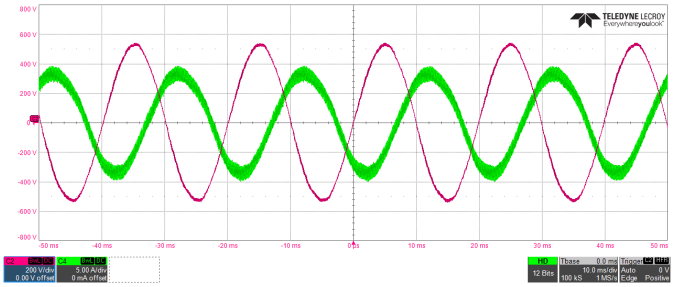

(b)

Fig. 6. Line to line voltage $v_{c,ab}$ and current $i_{g,a}$ waveforms during island operation: (a) with all loads connected; (b) without the NL load.

are inserted and their demand is satisfied by the grid. At t = 42.5 s, the circuit breaker opens and the inverter seamlessly provides the power requested by the loads. The total power reduces because of the reduction of the PCC voltage. Then, the converter properly follows the load changes over time. Moreover, it can be observed the correctness of the proportional frequency regulation.

Finally, Fig. 6 shows the waveforms of the line to line voltage $v_{c,ab}$ and the current $i_{g,a}$ during the island operation under two conditions: all loads connected (Fig. 6a); the non linear load is disconnected (Fig. 6b). It can be observed that the NL load introduces a non negligible harmonic distortion. Moverover, these pictures highlight a key feature of the S–VSC model: it imposes the current, not the voltage, even during

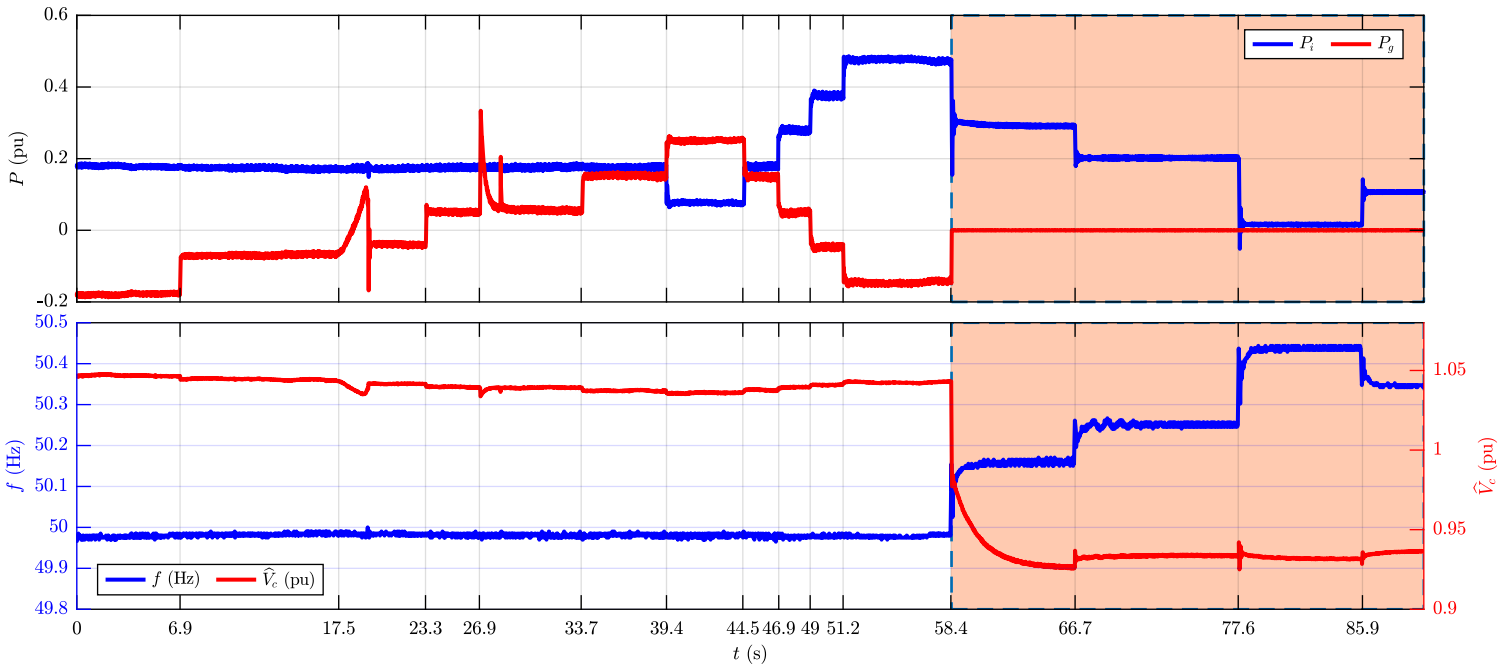

Fig. 7. Results of Test 2: (top) inverter power P_i (pu) and grid power P_g (pu) moving average trends; (bottom) S–VSC frequency f (Hz) and voltage amplitude $\widehat{V}_c$ (pu) trends.

island operation. Indeed, the voltage waveform is strongly affected by the requested current.

B. Test 2: Non–zero inverter external references

The results of Test 2 are proposed in Fig. 7 and commented in Table III. In the first part, the inverter external reference P_i^{ref} changes over time and the power requested by the loads is provided by both the grid and the inverter or only by the inverter, when sufficient. For instance, at $t = 49$ s the microgrid works in a self–consumption condition, in which all the loads demand is satisfied by the inverter. Then, at $t = 58.4$ s, the circuit breaker opens and the inverter must reduce the injected power, even if the external reference does not change, as for curtailment operation. The converter can only inject the power requested by the loads. If a storage system is added, the surplus of power can be used to charge it. Finally, even here, the frequency correctly follows the proportional droop law.

V. Conclusion

Virtual Synchronous Machines represent a promising solution to mitigate the future power system inertia reduction and the consequent stability issues. Moreover, the widespread of distributed energy resources can be facilitated by the diffusion of microgrids able to provide ancillary services and work both in grid–tied and island operation. Therefore, this paper has proposed an extended version of the S–VSC model to operate both as grid–tied and grid–forming converter, with no alteration on the performance already validated in previous works. Two experimental tests have demonstrated the grid–forming capability of the S–VSC model, representing a valid solution for the control of inverter–based MGs.

TABLE III
Events list of Test 2.

Time (s)	Comment
0	$P_i^{ref} = 0.2$ pu. The inverter injects power to the grid. $f \neq 50$ Hz $\Rightarrow P_d^* \neq 0 \Rightarrow P_i^* = P_d^* + P_i^{ref}$.
6.9	R Load insertion $\Rightarrow \Delta P_g = 0.1$ pu. The inverter satisfies the R load request and the remaing power is injected to the grid.
17.5	IM start up. The starter limits the inrush current.
23.3	10 Nm IM load insertion $\Rightarrow \Delta P_g = 0.1$ pu. The inverter provides part of the loads power. The remaing contribution is guaranteed by the grid.
26.9	NL load precharge.
33.7	NL load insertion $\Rightarrow \Delta P_g = 0.1$ pu. The inverter and the grid almost equally provide the loads power.
39.4	Inverter reference step $\Delta P_i^{ref} = -0.1$ pu $\Rightarrow$ $\Rightarrow \Delta P_g = 0.1$ pu.
44.5	Inverter reference step $\Delta P_i^{ref} = 0.1$ pu $\Rightarrow$ $\Rightarrow \Delta P_g = -0.1$ pu.
46.9	Inverter reference step $\Delta P_i^{ref} = 0.1$ pu $\Rightarrow$ $\Rightarrow \Delta P_g = -0.1$ pu.
49	Inverter reference step $\Delta P_i^{ref} = 0.1$ pu $\Rightarrow$ $\Rightarrow \Delta P_g = -0.1$ pu. The inverter provides all the power requested by the loads and the remaining term is injected to the grid.
51.2	Inverter reference step $\Delta P_i^{ref} = 0.1$ pu $\Rightarrow$ $\Rightarrow \Delta P_g = -0.1$ pu.
58.4	The circuit breaker is opened: Islanding $\Rightarrow P_g = 0$ pu. The inverter immediately provides only the loads power.
66.7	NL load disconnection $\Rightarrow \Delta P_i = -0.1$ pu.
77.6	IM torque inversion from 10 Nm to –10 Nm $\Rightarrow$ $\Rightarrow \Delta P_i = -0.2$ pu: the IM works as a generator and provides almost all the R load power.
85.9	IM torque load = 0 Nm $\Rightarrow \Delta P_i = 0.1$ pu: The inverter provides the power requested by the loads.

Future works on this topic will be focused on parallel inverters controlled both as an equivalent grid–forming converter and as a grid–forming and grid–feeding converters. Moreover, the behavior of the model under non ideal conditions and faults will be investigated.

REFERENCES

[1] R. Lasseter and P. Paigi, "Microgrid: a conceptual solution," in *2004 IEEE 35th Annual Power Electronics Specialists Conference (IEEE Cat. No.04CH37551)*, vol. 6, Jun. 2004, pp. 4285–4290 Vol.6, iSSN: 0275-9306.

[2] H. Jiayi, J. Chuanwen, and X. Rong, "A review on distributed energy resources and MicroGrid," *Renewable and Sustainable Energy Reviews*, vol. 12, no. 9, pp. 2472–2483, Dec. 2008. [Online]. Available: https://linkinghub.elsevier.com/retrieve/pii/S1364032107001025

[3] D. E. Olivares, A. Mehrizi-Sani, A. H. Etemadi, C. A. Cañizares, R. Iravani, M. Kazerani, A. H. Hajimiragha, O. Gomis-Bellmunt, M. Saeedifard, R. Palma-Behnke, G. A. Jiménez-Estévez, and N. D. Hatziargyriou, "Trends in microgrid control," *IEEE Transactions on Smart Grid*, vol. 5, no. 4, pp. 1905–1919, 2014.

[4] ENTSO-E, "High Penetration of Power Electronic Interfaced Power Sources and the Potential Contribution of Grid Forming Converters," Jan. 2020, Technical Report.

[5] ——, "Grid-Forming Capabilities: Towards System Level Integration," Mar. 2021, Technical Report.

[6] U. Tamrakar, D. Shrestha, M. Maharjan, B. P. Bhattarai, T. M. Hansen, and R. Tonkoski, "Virtual Inertia: Current Trends and Future Directions," *Applied Sciences*, vol. 7, no. 7, p. 654, Jul. 2017.

[7] M. Chen, D. Zhou, and F. Blaabjerg, "Modelling, Implementation, and Assessment of Virtual Synchronous Generator in Power Systems," *Journal of Modern Power Systems and Clean Energy*, vol. 8, no. 3, pp. 399–411, May 2020.

[8] V. Mallemaci, F. Mandrile, S. Rubino, A. Mazza, E. Carpaneto, and R. Bojoi, "A Comprehensive Comparison of Virtual Synchronous Generators with Focus on Virtual Inertia and Frequency Regulation," *Electric Power System Research, Elsevier*, 2021, in Press.

[9] H. Beck and R. Hesse, "Virtual synchronous machine," in *2007 9th International Conference on Electrical Power Quality and Utilisation*, 2007, pp. 1–6.

[10] S. Rubino, A. Mazza, G. Chicco, and M. Pastorelli, "Advanced control of inverter-interfaced generation behaving as a virtual synchronous generator," in *2015 IEEE Eindhoven PowerTech*, Jun. 2015, pp. 1–6.

[11] M. Blau and G. Weiss, "Synchronverters used for damping inter-area oscillations in two-area power systems," *Renewable Energy and Power Quality Journal*, pp. 45–50, 04 2018.

[12] P. Lorenzetti, Z. Kustanovich, S. Shivratri, and G. Weiss, "The equilibrium points and stability of grid-connected synchronverters," 2021.

[13] P. Rodriguez, I. Candela, and A. Luna, "Control of pv generation systems using the synchronous power controller," in *2013 IEEE Energy Conversion Congress and Exposition*, 2013, pp. 993–998.

[14] W. Zhang, A. Luna, I. Candela, J. Rocabert, and P. Rodriguez, "An active power synchronizing controller for grid-connected power converters with configurable natural droop characteristics," in *2015 IEEE 6th International Symposium on Power Electronics for Distributed Generation Systems (PEDG)*, 2015, pp. 1–7.

[15] K. Sakimoto, Y. Miura, and T. Ise, "Stabilization of a power system with a distributed generator by a virtual synchronous generator function," in *8th International Conference on Power Electronics - ECCE Asia*, 2011, pp. 1498–1505.

[16] S. D'Arco, J. A. Suul, and O. B. Fosso, "Control system tuning and stability analysis of virtual synchronous machines," in *2013 IEEE Energy Conversion Congress and Exposition*, 2013, pp. 2664–2671.

[17] F. Mandrile, E. Carpaneto, and R. Bojoi, "Virtual synchronous generator with simplified single-axis damper winding," in *2019 IEEE 28th International Symposium on Industrial Electronics (ISIE)*, 2019, pp. 2123–2128.

[18] F. Mandrile, E. Carpaneto, and R. Bojoi, "Vsg simplified damper winding: Design guidelines," in *IECON 2019 - 45th Annual Conference of the IEEE Industrial Electronics Society*, vol. 1, 2019, pp. 3962–3967.

[19] ——, "Grid-tied inverter with simplified virtual synchronous compensator for grid services and grid support," in *2019 IEEE Energy Conversion Congress and Exposition (ECCE)*, 2019, pp. 4317–4323.

[20] ——, "Grid-Feeding Inverter With Simplified Virtual Synchronous Compensator Providing Grid Services and Grid Support," *IEEE Transactions on Industry Applications*, vol. 57, no. 1, pp. 559–569, Jan. 2021.

[21] F. Mandrile, D. Cittanti, V. Mallemaci, and R. Bojoi, "Electric Vehicle Ultra-Fast Battery Chargers: A Boost for Power System Stability?" *World Electric Vehicle Journal*, vol. 12, no. 1, p. 16, Mar. 2021, number: 1 Publisher: Multidisciplinary Digital Publishing Institute. [Online]. Available: https://www.mdpi.com/2032-6653/12/1/16

[22] F. Mandrile, V. Mallemaci, E. Carpaneto, and R. Bojoi, "A Lead-Lag Filter for Virtual Synchronous Machines with Improved Electromechanical Damping," *2021 IEEE Energy Conversion Congress and Exposition (ECCE)*, 2021, in Press.

[23] P. Kundur, *Power System Stability and Control.* McGraw-Hill Education, Jan. 1994, ISBN: 978-0-07-035958-1.

[24] F. Mandrile, E. Carpaneto, E. Armando, and R. Bojoi, "Simple tuning method of virtual synchronous generators reactive control," in *2020 IEEE Energy Conversion Congress and Exposition (ECCE)*, 2020, pp. 2779–2785.